The Cytosensor Microphysiometer: Biological Applications of Silicon Technology

H. M. McConnell, J. C. Owicki, J. W. Parce,* D. L. Miller, G. T. Baxter, H. G. Wada, S. Pitchford

A silicon-based device, dubbed a microphysiometer, can be used to detect and monitor the response of cells to a variety of chemical substances, especially ligands for specific plasma membrane receptors. The microphysiometer measures the rate of proton excretion from 10^4 to 10^6 cells. This article gives an overview of experiments currently being carried out with this instrument with emphasis on receptors with seven transmembrane helices and tyrosine kinase receptors. As a scientific instrument, the microphysiometer can be thought of as serving two distinct functions. In terms of detecting specific molecules, selected biological cells in this instrument serve as detectors and amplifiers. The microphysiometer can also investigate cell function and biochemistry. A major application of this instrument may prove to be screening for new receptor ligands. In this respect, the microphysiometer appears to offer significant advantages over other techniques.

The best known applications of silicon (Si) technology are in nonbiological realms, such as computers. This article, however, describes a biological application of Si technology: the integration of living cells with a Si-based sensor to form an instrument that detects a wide variety of molecules in the cells' environment by effects on cell physiology.

This instrument is called the microphysiometer (its manufactured version is the Cytosensor), and it differs from most other analytical instruments. Instead of reporting structural features of an analyte as do, for example, electrophoresis, nuclear magnetic resonance, and immunoassays, the microphysiometer instead reports the effects of an analyte on biological function. In other words, it is a system for performing bioassays. It is more akin to techniques that monitor cell growth and morphology, assays of biochemical change, and techniques that measure variations in transmembrane potentials and currents.

With few exceptions, cells acidify their environments because of acidic products of energy metabolism. Adenosine triphosphate (ATP) production by means of energy metabolism is tightly coupled to cellular ATP consumption such that changes in cell physiology cause changes in the rate of energy use and, hence, in the rate of extracellular acidification. In many cases, these changes are large enough to detect conveniently with the microphysiometer; typically, changes of 10 to 100% occur on a time scale of seconds to minutes. Another kind of proton-mediated signal of physiological changes arises from changes in intracellular pH, which appear as complementary changes in extracellular pH as protons are transported across the plasma membrane. These effects are the bases of the broad applicability of the instrument.

The microphysiometer uses a light-addressable potentiometric sensor (LAPS) to measure the rate at which cells acidify their environment. Figure 1 is a diagram of the LAPS and its accompanying circuitry. The LAPS is a piece of doped Si with a thin insulator on the surface. An external circuit connects an ohmic contact on the Si to an aqueous compartment that is in contact with the insulator. The function of the external circuit is twofold. It controls the potential from the Si to the aqueous solution and measures an alternating photocurrent. The photocurrent is generated when the sensor is illuminated with an amplitude-modulated light-emitting diode (LED). When the potential from Si to solution is adjusted so that the Si is forward biased, no photocurrent flows in the external circuit. When the sensor is reverse biased, a voltage gradient (depletion layer) is formed immediately below the insulator. This voltage gradient results in the separation of hole-electron pairs formed by absorption of light from the LED, and an ac-coupled photocurrent flows in the external circuit. No direct current passes through the insulator.

The applied potential (Ψ) at which photocurrent begins to flow is defined by the sum of a variety of constant potentials (that is, contact potentials) and the surface potential of the aqueous-insulator interface. Changes in the surface potential can therefore be measured by a determination of the changes in Ψ required to produce a photocurrent. The surface of the Si nitride insulator contains hydroxyl and amino functions, both of which can be titrated as a function of pH. Therefore, the surface potential at the aqueous-insulator interface is sensitive to pH. A properly prepared Si nitride surface has a sufficiently high density of titratable groups to make the pH response of the surface potential Nernstian (61 mV per pH unit at 37°C). The light-addressable nature of the sensor results from the fact that the pH is measured only at the site of illumination by the LED. Other devices have used this feature to perform several immunoassays simultaneously on one sensor (*1*). In the Cytosensor, only one LED is used

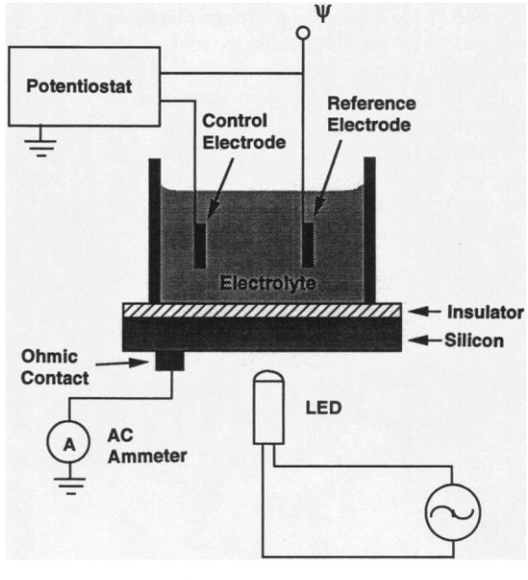

Fig. 1. Schematic drawing of the light-addressable potentiometric sensor (LAPS).

H. M. McConnell is in the Department of Chemistry, Stanford University, Stanford, CA 94305 and is a director at Molecular Devices Corporation, 4700 Bohannan Drive, Menlo Park, CA 94025. J. C. Owicki, J. W. Parce, D. L. Miller, G. T. Baxter, H. G. Wada and S. Pitchford are at Molecular Devices Corporation, 4700 Bohannon Drive, Menlo Park, CA 94025.

*To whom correspondence should be addressed.

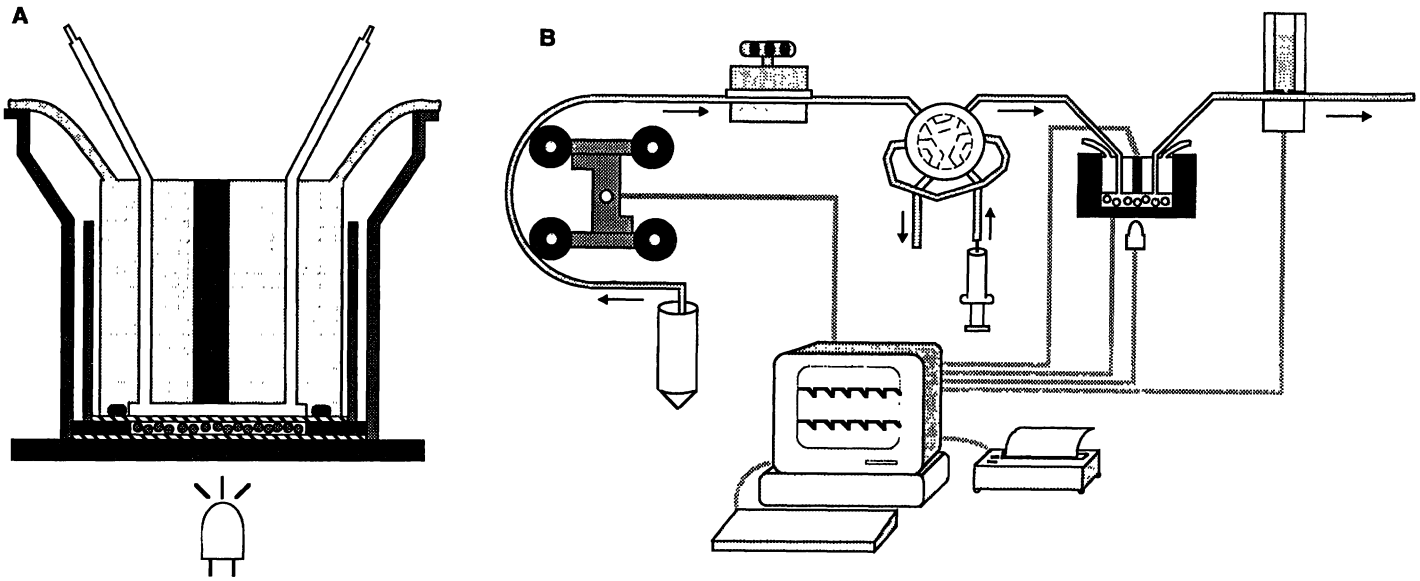

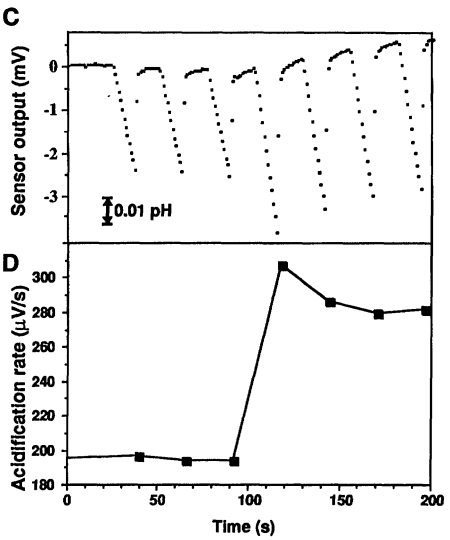

Fig. 2. Cytosensor description and operation. (**A**) Flow chamber containing cells. Cells are retained in a disk-shaped region 50 μm high and 6 mm in diameter between two track-etched microporous polycarbonate membranes, shown with diagonal hatching. The sensing surface (top) of the LAPS contacts the lower membrane, and culture medium flows tangentially across the surface of the upper membrane. An LED (bottom of figure) illuminates the non-sensing surface (bottom) of the LAPS. (**B**) Instrumentation schematic. The electronics that operates the LAPS makes three analog connections to the instrument beyond those to the LED: one to the underside of the LAPS chip, one to a controlling electrode in the ceiling of the flow chamber, and one to the reference electrode. A complete Cytosensor system contains eight flow chambers and associated components managed by one computer. (**C**) Plot of pH versus time for CHO cells transfected with the muscarinic acetylcholine receptor. Agonist (carbachol) was added at time t = 100 s. (**D**) Plot of acidification rate versus time for the data shown in (C). During each flow-off period shown in (C), the sensor data are fit to a straight line with the use of a least-squares procedure; the slope of this line is reported as the acidification rate. Numerically, 1 μV/s is close to 1 × 10^{-3} pH units per minute. In this figure, receptors on the cells were activated with an agonist midway through the period shown. The increase in acidification rate is apparent.

per sensor chamber. In this configuration, it is possible to optimize the signal-to-noise ratio of the pH measurement. At present, the instrument makes one pH reading per second in every chamber with a root-mean-square noise between 0.0005 and 0.001 pH units. This low noise feature of the LAPS is very important for the measurement of subtle changes in cell physiology in the microphysiometer.

The following paragraphs provide a more detailed description of the physical and biochemical aspects of the microphysiometer. Additional information about the LAPS can be found in (*2*); additional information about the operation of the microphysiometer can be found in (*3*) and (*4*). For a thorough discussion of quantitative aspects of cellular metabolism relative to microphysiometry, see (*5*) and references therein. We conclude with some examples of applications of the microphysiometer.

The Microphysiometer and Its Biological Basis

Cells, whether eukaryotic or prokaryotic, adherent or nonadherent, are retained by the microphysiometer in a flow chamber in aqueous diffusive contact with the pH-sensitive surface of a LAPS chip (Fig. 2A). Adherent cells attach directly to the membrane surface, whereas nonadherent cells are immobilized by, for example, entrapment within a fibrin clot. An infrared LED illuminates the underside of the LAPS chip, which defines the region of the chamber from which data are obtained. As shown in Fig. 2B, this chamber is the heart of an instrument that controls the flow of medium over the cells, the introduction of test substances, the chamber temperature, the LAPS electronics, and data management. Culture medium is pumped from a reservoir by a peristaltic pump and passes through a debubbler-degasser, a selection valve, and the flow chamber. After leaving the flow chamber, it passes a reference electrode en route to a waste receptacle. Samples for analysis can be introduced at the selection valve through an injection loop. Alternately, the tubing can be configured so that the valve controls which of two pumped streams of media enters the flow chamber. A personal computer (a Macintosh with dedicated software) controls the LAPS electronics, the pump, and the valve; it also manages data acquisition, analysis, and storage.

The extracellular acidification rate is determined by measurement of the decrease in pH that occurs as acidic metabolites build up during brief halts in the flow of media (Fig. 2, C and D). Once each second for each flow chamber, the LAPS makes a voltage measurement that is linearly related to pH (a decrease of 61 mV is approximately equal to an acidification of 1 pH unit at 37°C). During fluid flow, the sensor output is stable and reflects a pH near that of the culture medium entering the flow chamber. When the flow is briefly halted, typically for 30 to 60 s, the pH in the chamber decreases as a result of the excretion of protons by the cells. These acidifications are typically <0.1 pH unit and cause no significant perturbations of cell physiology. When the flow is resumed, the sensor output rises to the previous steady state as the mildly acidified medium is flushed out. The flow cycle is repeated continually, yielding one

measurement of acidification rate at each flow-off period. Usually, one can improve the sensitivity of the method by decreasing the buffer capacity of the culture medium to about 1 mM per pH unit by not adding strongly buffering species such as bicarbonate and Hepes to the medium.

Figure 3 shows schematically the principal cellular mechanisms by which protons are produced and excreted for a composite mammalian cell with the use of glucose as a carbon source. It further indicates how these processes can be modulated by ligand-receptor interactions, as discussed below. The main parts of the proton economy include several factors.

Proton production. Glucose enters through a glucose transport protein and is metabolized to lactic acid by glycolysis or oxidized to CO_2 by respiration. At physiological pH, both of these weak acids are predominantly dissociated.

Proton excretion. These protons cross the plasma membrane by several means, both unfacilitated and facilitated. Some of the lactic acid and CO_2 passively diffuses across the membrane. Lactic acid is also excreted through the monocarboxylic acid transporter. Bicarbonate exits by several varieties of anion transport proteins, one of which is shown (Fig. 3). Pathways for proton efflux include the Na^+-H^+ exchanger as well as various proton channels and pumps.

Regulatory mechanisms and receptor activation. Energy metabolism is largely regulated by cellular demand for ATP, which arises from diverse metabolic processes. In Fig. 3, the maintenance of transmembrane Na^+-K^+ gradients by means of Na^+, K^+-dependent adenosine triphosphatase is shown. The activation of a receptor can alter the rate of extracellular acidification by causing metabolic changes that affect demand for ATP. It can also act more directly at key regulatory points such as the Na^+-H^+ exchanger and glucose transport.

For a typical cultured mammalian cell such as a fibroblast, energy metabolism yields $\sim 10^8$ protons per second in steady state. Table 1 shows that the metabolism of all of the carbon sources commonly used in mammalian cell culture media leads to acidification. Glycolysis is by far the most acidifying process in terms of protons produced per turnover of an ATP molecule. Coupled to the fact that glycolysis is usually very active in cultured cells (in contrast to in vivo), this means that most of the protons excreted by cultured cells are usually of glycolytic origin. Data obtained with the microphysiometer to corroborate this are shown in Fig. 4A. Chinese hamster ovary–K1 (CHO-K1) cells maintained on glucose show high acidification rates that decrease significantly when the glucose is replaced by pyruvate or is simply removed from the medium.

The overshoot that occurs when pyruvate is replaced by glucose is evidence of a feature of the transport mechanisms of monocarboxylic acids: the ionized form cannot permeate a membrane, but the protonated form can be transported either by the monocarboxylic acid carrier or by unfacilitated diffusion. The addition of such weak acids extracellularly causes a pulse of alkalinization that is the result of the influx of the protonated form until transmembrane equilibrium is reached. The removal of the weak acid causes a pulse of acidification as the process is reversed. This effect is shown more clearly in Fig. 4B with oxamate, a nonmetabolizable analog of pyruvate.

The Na^+-H^+ exchange protein in the plasma membrane is an important and dynamically controlled regulatory mechanism for intracellular pH. The activity of this antiporter can be observed directly in the microphysiometer (Fig. 4C). Cells are incubated in media in which Na^+ is replaced with choline, which starves the Na^+-H^+

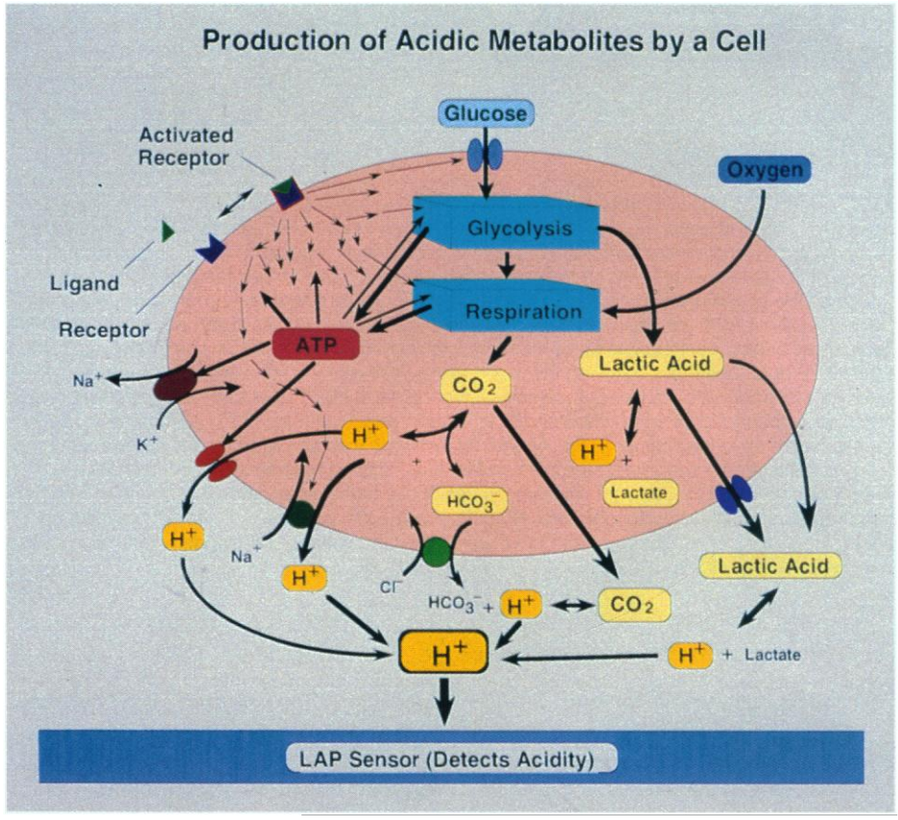

Fig. 3. The cell biology of extracellular acidification. The figure schematically shows the main features of cellular proton economy. Not all cells use all of the pathways shown in this composite figure.

Table 1. Proton yield per ATP molecule turned over during energy metabolism of representative carbon sources. ATP does not appear explicitly in the reactions because it was assumed that ATP synthesis and hydrolysis are tightly coupled. Because hydrolysis of one ATP molecule per second produces a substantial fraction of a proton, imbalances between ATP synthesis and hydrolysis can produce transient alterations in the rate of acidification.

Carbon source	Pathway	Reaction	ATP yield (per substrate molecule)	H^+ per ATP molecule
Glucose	Glycolysis	Glucose $\rightarrow$ 2 lactate$^-$ + 2 H^+	2	1.000
Glucose	Respiration	Glucose + 6 O_2 $\rightarrow$ 6 HCO_3^- + 6 H^+	36	0.167
Glutamine	Respiration	Glutamine + 9/2 O_2 + 3 H_2O $\rightarrow$ 5 HCO_3^- + 2 NH_4^+ + 3 H^+	27	0.111
Pyruvate	Respiration	Pyruvate$^-$ + 5/2 O_2 + H_2O $\rightarrow$ 3 HCO_3^- + 2 H^+	15	0.333

exchanger and causes an increase in intracellular proton concentration. When choline is replaced with Na^+, a large surge of extracellular acidification accompanies the reestablishment of homeostasis. This surge is nearly abolished by amiloride, an inhibitor of the Na^+-H^+ exchange system.

Applications

One of the major driving forces leading to the construction of the microphysiometer was the possibility of observing functional ligand receptor interactions by the monitoring of cellular metabolic rates. We have now demonstrated substantial cellular metabolic consequences that are the result of the triggering of a wide variety of receptors (Table 2). In the vast majority of ligand receptor combinations tested to date, functional receptor agonist interactions result in an increase in cellular acidification rates. There are some cases, however, where the opposite is true (6).

Table 2. Representative receptors for which acidification responses to triggering have been demonstrated in the microphysiometer. The table indicates the receptor, the superfamily to which the receptor belongs and the second messenger pathway activated by the receptor, whether the response was derived from receptors native to the cells or whether the response was derived from receptors transfected into the cells, and citations for the data. N.D., not done.

Receptor	Superfamily, pathway	Native	Transfected	Reference
m1 Muscarinic acetylcholine	G protein, inositol phosphate	N.D.	Yes	(*11*)
Muscarinic, subtype unknown	G protein	Yes	N.D.	(*18*)
β_2-Adrenergic	G protein, increasing cAMP	N.D.	Yes	(*11*)
Prostaglandin E	G protein, increasing cAMP	Yes	N.D.	(*19*)
Dopamine D1	G protein, increasing cAMP	No	Yes	(*20*)
Dopamine D2	G protein, decreasing cAMP	No	Yes	(*20, 21*)
Glutamate (kainate)	Excitatory amino acid, ion channel	Yes	N.D.	(*15*)
Insulin, insulin-like growth factor	Growth factor, tyrosine kinase	Yes	N.D.	(*22*)
Epidermal growth factor	Growth factor, tyrosine kinase	Yes	Yes	(*3, 11, 14*)
γ-Interferon	Hematopoietin	Yes	N.D.	(*23*)
Interleukin-2	Hematopoietin	Yes	N.D.	(*14*)
Interleukin-4	Hematopoietin	Yes	N.D.	(*23*)
GM-CSF	Hematopoietin	Yes	N.D.	(*8*)
T cell	T cell receptor	Yes	N.D.	(*14*)

Both the magnitude and the kinetics of the response depend on a variety of factors, including the type of receptor, the type of cell in which the receptor resides, the concentration of agonist, and the pretreatment of the cells before the introduction of agonist (*7*). Variations in the amplitude and kinetics of the cellular response as a function of different concentrations of granulocyte-macrophage colony-stimulating factor (GM-CSF) are illustrated in Fig. 5A. This response profile is typical of those receptors that affect cell proliferation. Low concentrations of agonist result in a gradual low-amplitude increase in acidification rate. As the agonist concentration is increased, the acidification amplitude increases and the time to reach the point of maximum acidification decreases. For the GM-CSF receptor, this response has been resolved into two components (*8*). The rapid component is a result of the activation of the Na^+-H^+ antiporter, and the slower is a result of the stimulation of glycolysis (*9*).

The diversity of responses obtained when different receptors are triggered is illustrated in Fig. 5B. The muscarinic acetylcholine (carbachol) response has a very rapid, transient component, and the maximum acidification rate is reached about 30 s after introduction of the agonist. The response decays rapidly thereafter, reaching a new plateau within a few minutes. In contrast, the response to nerve growth factor (NGF) reaches a maximum in a time that is approximately an order of magnitude longer and remains elevated for an extended peri-

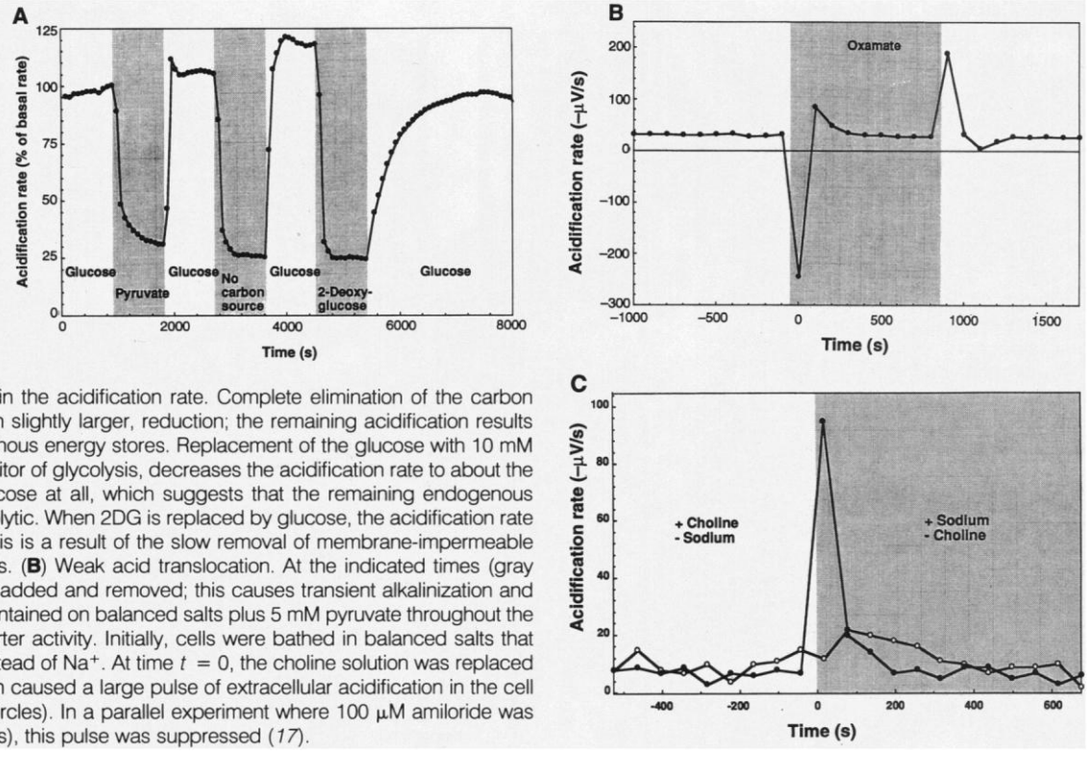

Fig. 4. Mechanisms of extracellular acidification. CHO-K1 cells were maintained in the microphysiometer in balanced salts plus the indicated carbon source. (**A**) Dependence of acidification rate on the carbon source. The replacement of 10 mM glucose by 10 mM pyruvate causes a rapid reduction in the acidification rate, which is rapidly reversible. These cells can use pyruvate as an energy source; the addition of pyruvate to glucose-containing medium also causes a significant decrease in the acidification rate. Complete elimination of the carbon source causes a similar, though slightly larger, reduction; the remaining acidification results from the metabolism of endogenous energy stores. Replacement of the glucose with 10 mM 2-deoxyglucose (2DG), an inhibitor of glycolysis, decreases the acidification rate to about the same level as that with no glucose at all, which suggests that the remaining endogenous metabolism is not strongly glycolytic. When 2DG is replaced by glucose, the acidification rate recovers slowly. Presumably, this is a result of the slow removal of membrane-impermeable 2DG-6-phosphate from the cells. (**B**) Weak acid translocation. At the indicated times (gray shading), 20 mM oxamate was added and removed; this causes transient alkalinization and acidification. The cells were maintained on balanced salts plus 5 mM pyruvate throughout the experiment. (**C**) Na^+-H^+ antiporter activity. Initially, cells were bathed in balanced salts that contained choline (130 mM) instead of Na^+. At time $t = 0$, the choline solution was replaced by normal balanced salts, which caused a large pulse of extracellular acidification in the cell chamber (denoted by closed circles). In a parallel experiment where 100 μM amiloride was present throughout (open circles), this pulse was suppressed (*17*).

od. A similar response rise time is observed for GM-CSF, but this response decays somewhat even in the continued presence of cytokine.

One task in the evaluation of potential pharmaceutical compounds is the determination of the efficacious concentration of the compound of interest. For receptor ligands, this is typically done with the introduction of the ligand to the cells at various concentrations and the measurement of the subsequent cellular response by biochemical assays for intermediates of second messenger pathways known to be activated by the receptor of interest. These experiments result in a dose-response curve that yields a characteristic concentration at which 50% of the maximal response is obtained (EC_{50}). Analogous experiments can be carried out in the microphysiometer. An example of the generation of a dose-response curve for a receptor agonist pair is given in Fig. 6. Here, the receptor is the rat m1 muscarinic acetylcholine receptor and the agonist is the nonhydrolyzable acetylcholine analog carbamylcholine (carbachol). The EC_{50} value for carbachol derived from this experiment is ~2 μM, which is in good agreement with the value of ~5 μM obtained by measurement of the phosphatidyl inositol hydrolysis as a function of carbachol concentration in the same cell line (*10*). We have previously reported the EC_{50} determined on the microphysiometer for triggering β-adrenergic receptors with isoproterenol (*11*). This value also compares favorably with values obtained with the use of adenosine 3′,5′-monophosphate (cAMP) measurements for the same receptor-ligand combination.

Because the acetylcholine receptor desensitizes with continued exposure to an agonist, it is necessary to limit exposure of the cells to the minimum time required to obtain a response if the same chamber of cells is to be used in order to generate the entire dose-response curve. An alternative approach is to place the cells in a set of chambers in parallel and expose them in each chamber to a different concentration of agonist. Although this approach is less efficient with regard to throughput, it is necessary for some receptor types. In the case of many of the growth factor receptors we have examined, the elevated metabolic response to a short bolus of growth factor may last for more than 1 hour (Figs. 5A and 7B). Under these conditions, the generation of dose-response curves by sequential addition of agonist to the same chamber of cells becomes impractical.

Figure 7 illustrates experiments designed to investigate second messenger pathways with the microphysiometer. Genistein inhibits tyrosine kinase activity. This effect is illustrated in Fig. 7A, where acidification that is the result of the triggering of the NGF receptor is inhibited by about 35% by typical inhibitory concentrations of genistein. The experiment illustrated in Fig. 7B was designed to determine which of several isoforms of protein kinase C is involved in the second messenger pathway triggered by GM-CSF receptors. Synthetic

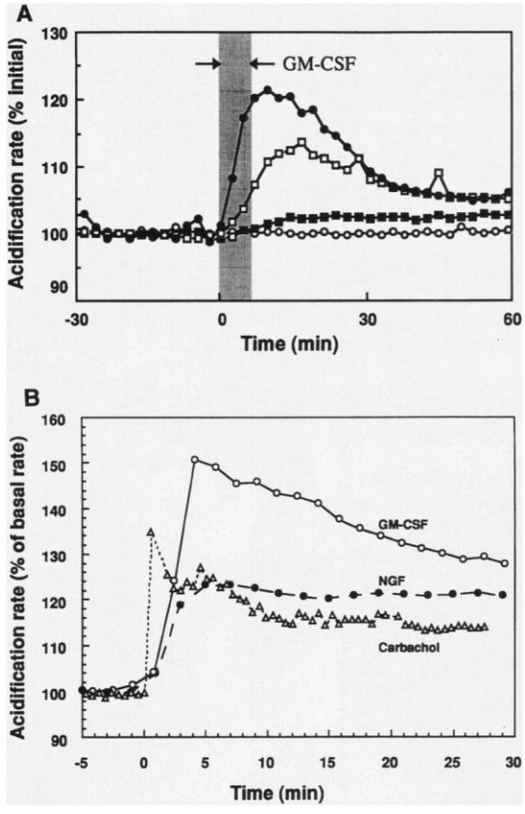

Fig. 5. Diversity of receptor responses to receptor activation. (**A**) Response versus ligand concentration. Cells from the human bone marrow cell line, TF-1, were loaded in four microphysiometer chambers. The cytokine GM-CSF was added to a final concentration of 0 ng/ml (open circles), 0.1 ng/ml (closed squares), 1 ng/ml (open squares), or 10 ng/ml (closed circles) during the period indicated by the shaded region. The acidification rates were all normalized to the average rate before the addition of cytokine. (**B**) Response characteristics of different receptors. The response of TE-671 rhabdomyosarcoma cells to 1 mM carbachol is rapid and multiphasic, and the multiphasic character of the response is reproducible. The responses of the PC-12 cells to NGF (100 ng/ml) and the response of TF-1 cells to GM-CSF (10 ng/ml) are an order of magnitude slower. The latter two responses differ in that the response to NGF is constant during a 30-min period whereas the response to GM-CSF decays to about 40% of maximum in a 30-min period.

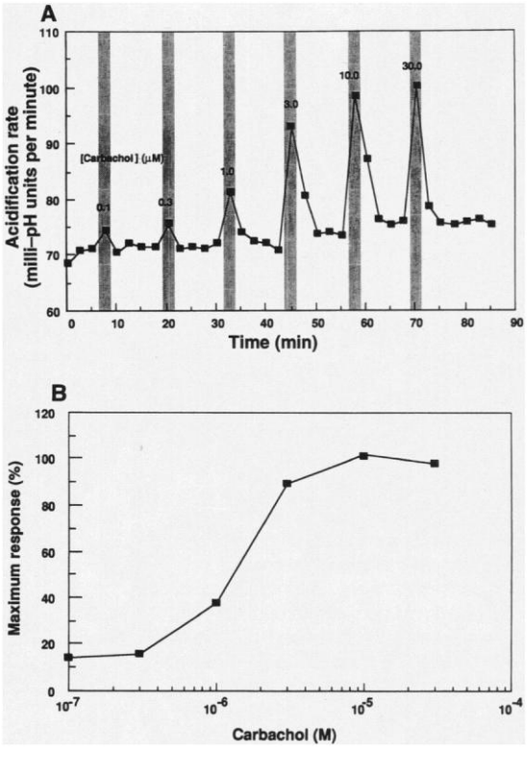

Fig. 6. Carbachol dose-response of CHO cells transfected with an m1 muscarinic acetylcholine receptor. (**A**) Extracellular acidification for sequential additions of increasing concentrations of carbachol. The transfected CHO cells were placed in the microphysiometer, and acidification rates were monitored every 2.5 min. Carbachol was introduced to the cells at the concentrations indicated in the figure for one measurement cycle per concentration (gray bars). (**B**) Amplitude of peak response versus carbachol concentration. The difference between acidification rate in the presence of carbachol and that immediately before each addition of carbachol was calculated, normalized to 100% for the largest response, and plotted as a function of carbachol concentration.

antisense DNA specific for the ε isoform (and not the α isoform) was found to inhibit significantly the acidification response. The antisense treatment was demonstrated to diminish specifically the levels of the appropriate isoform by protein immunoblot analysis with isoform-specific antibodies (*12*).

Infection of cells with viruses often leads to major changes in cellular metabolism and eventually cell death. These metabolic changes can be monitored continuously in the microphysiometer. Figure 8A shows the effect of vesicular stomatitis virus (VSV) infection on the acidification rates of mouse fibroblasts (L cells). The control cells show a constant increase in acidification rate during the course of the experiment as a result of their normal rate of proliferation in the cell chamber. The addition of high concentrations of virus [ten plaque-forming units per L cell, or a multiplicity of infection (MOI) of 10] results in a decrease in the normal proliferative rate that can be seen in the first few hours. This is followed by a precipitous decline in acidification rate at ~9 hours after infection. As the effective dose of virus is decreased, the early effects on metabolic rate are decreased, and the time after infection at which the precipitous drop in acidification rate occurs is increasingly longer. The latter effect reflects the need for the virus to go through more replication cycles in order to infect the majority of the cells.

In contrast to the kinetics of VSV infection, the effect of human immunodeficiency virus–1 (HIV-1) infection on the acidification rate of CD4-transfected HeLa cells does not become apparent until several days after infection. Figure 8B shows the effect of administration of various concentrations of AZT (azidothymidine) on HIV-1–infected HeLa cells. The data are presented as the ratio of the acidification rates of infected cells to the acidification rates of uninfected cells. This is done to simplify the plot because the acidification rate of the uninfected cells increases over the 6-day period because of significant cell growth in the flow chambers. Microscopic examination of the infected cells removed from the cell chamber with no AZT on day 5 showed significant cytopathology, including the formation of syncytia that stained positive with antibodies to HIV (*13*). The general high sensitivity of acidification rate to cell physiology suggests that the microphysiometer may be used to screen for antiviral agents.

Conclusion

In general, robust acidification responses are observed for two large classes of receptors: the family of receptors with seven transmembrane helices (seven-helix) and the tyrosine kinase receptor family. Members of the seven-helix family studied include the β_2-adrenergic receptor and the m1 muscarinic acetylcholine receptor. The triggering of the β-adrenergic receptor by

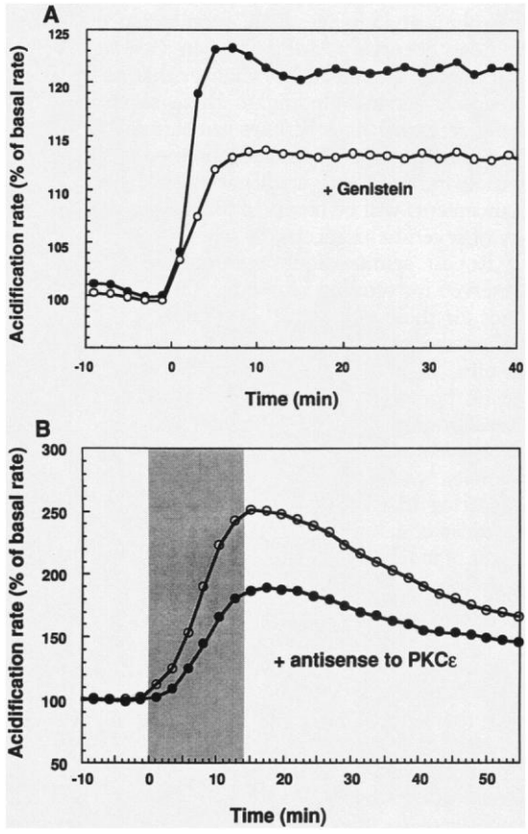

Fig. 7. Modulating second messenger pathways. (**A**) Effect of inhibiting tyrosine kinase activity on acidification response to NGF. PC-12 neuroblastoma cells were placed in two microphysiometer chambers. The medium that supplied the cells contained no additions (closed circles) or genistein (25 μg/ml) (open circles). NGF (100 ng/ml) was added at $t = 0$. (**B**) Effect of inhibition of protein kinase Cε (PKCε) activity on the acidification response to GM-CSF. TF-1 cells were maintained in culture for 9 days in the presence (closed circles) or absence (open circles) of 15 μM PKCε-antisense oligonucleotide. Cells were placed in the microphysiometer and triggered with GM-CSF (5 ng/ml) at $t = 0$.

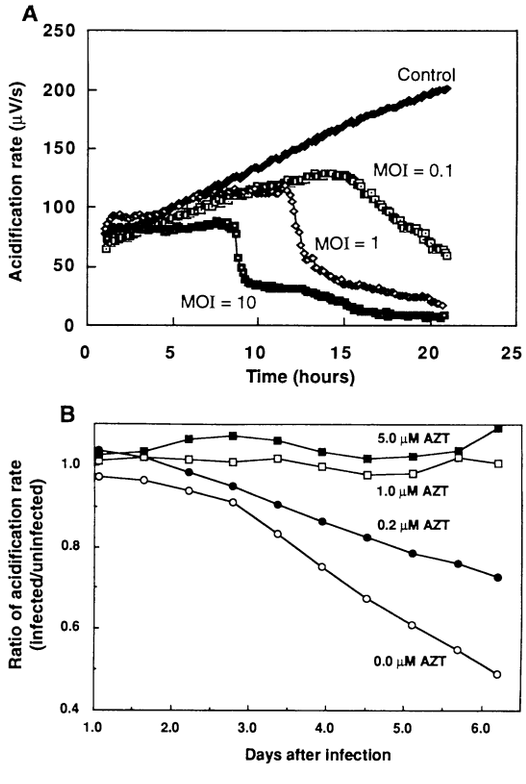

Fig. 8. Detection of viral cytopathology by the microphysiometer. (**A**) Effect of virus concentration. Mouse 929 L cells were incubated with the Indiana strain of VSV at an MOI of 0 (control), 0.1, 1, or 10 for 30 min at 5°C beginning at $t = 0$. The acidification rate of the cells was monitored in the microphysiometer at 37°C. (**B**) AZT inhibition of HIV-1 cytopathology. CD4-transfected HeLa cells were incubated with HIV-1 at an MOI of 1 for 1 hour at 37°C. The cells were then placed in the microphysiometer, and acidification rates were monitored for 6 days in four parallel chambers. The medium that flowed through the chambers contained AZT at the concentrations indicated in the figure. Acidification rates in (B) are presented as the ratio of the acidification rates of infected cells to those of uninfected cells.

epinephrine brings about a biochemical cascade that involves G proteins, adenylate cyclase, and protein kinase. The m1 muscarinic acetylcholine receptor also uses a G protein but stimulates phosphatidyl inositol hydrolysis and changes in K^+ conductance and can decrease cAMP levels. In view of the extensive biochemical changes that accompany agonist binding to these seven-helix receptors, it is perhaps not surprising that enhanced acidification is observed. We anticipate that large acidification rate enhancements will be observed for the majority of seven-helix receptors.

Robust acidification responses are also observed for tyrosine kinase receptors. Ligands for these receptors that result in such enhancements of acidification rates include insulin, epidermal growth factor, NGF, acidic fibroblast growth factor, GM-CSF, transforming growth factor–α, and complexes between major histocompatibility complex protein and peptide (*14*). The triggering of these receptors also leads to cascades of cellular biochemical events. In terms of monitoring the triggering of seven-helix receptors and tyrosine kinase receptors as well as screening for new receptor agonists, the microphysiometer appears to offer an efficient, convenient approach. The percentage increase in acidification rate that is the result of the triggering of many of these receptors is particularly large in the presence of glucose, which suggests a close linkage between receptor triggering and glycolysis (*8*).

A third category of receptors is the ligand-gated ion channels; examples include the nicotinic acetylcholine receptor and various glutamate receptors. The triggering of nicotinic acetylcholine receptors has not yet been detected with the Cytosensor; order-of-magnitude estimates of the ATP consumption required to pump out Na^+ ions after the triggering of this rapidly desensitizing receptor suggest that the resulting acidification may be close to the detection limit. There are a number of distinct glutamate receptors, as defined by the actions of various agonists. The triggering of the kainate (glutamate) receptor in fetal rat hippocampal neurons gives large responses in the microphysiometer (*15*).

The Cytosensor can be used to detect and analyze the triggering of a wide variety of plasma membrane receptors. It is thus of interest to consider possible applications of this instrumentation in basic research and in biotechnology. At present, it appears that the Cytosensor is ideal for screening for ligands of orphan receptors. Orphan receptors are putative receptors for which the specific ligands are not known. The β_3-adrenergic receptor may be an example of an orphan receptor of the seven-helix type. Many oncogene tyrosine kinases form a large class of orphan receptors; an example of a recently identified ligand of a tyrosine kinase receptor is heregulin, an activator of $p185^{erbB2}$ (*16*). It is likely that the sequencing of the human genome will uncover a large number of orphan receptors. Toward the discovery of the receptor ligands, it will be convenient to compare the responses of receptor-positive and otherwise identical receptor-negative cells (*11*). It should be possible to carry out such experiments with receptor-positive cells that have transient receptor transfections because the Cytosensor permits rapid bioassays to be made during the lifetime of the transfection. In some cases, the choice of the receptor-negative cell should be straightforward, but in other cases cotransfection of membrane-associated proteins, such as products of oncogenes, may be necessary.

Given a source of potential orphan receptor ligands, such as cell culture supernatants, the Cytosensor appears to have advantages over other instruments and methods for screening for these ligands. A conventional procedure for the discovery of new agonists and antagonists involves the displacement of radioactive ligands bound to plasma membrane receptors. This approach is obviously inapplicable in this case. Fluorometric detection of Ca^{2+} influx or release that is the result of ligand-receptor binding will miss cell triggering events that do not lead to changes in cytosolic Ca^{2+} concentration. [For example, the triggering of TF-1 cells by GM-CSF does not lead to a change in cytosolic Ca^{2+} concentration (*12*).] Changes in the state of membrane protein and cytosolic protein phosphorylation could undoubtedly be used to detect cell triggering by receptor ligands. However, it is difficult to imagine how this method could be used for large-scale screening in view of the radioactivity required or the associated tedious biochemical assays, or both. Inconvenience and lack of applicability for large-scale screening also apply to measurements of transmembrane potentials. Microphysiometers can be used quite generally to detect the triggering of a large number of plasma membrane receptors by specific ligands. This technique for the detection of cell triggering may have broad applicability in biotechnology and basic research in cell biology and may be particularly well suited to screen for the ligands of orphan receptors.

REFERENCES AND NOTES

1. J. Briggs and P. R. Panfili, *Anal. Chem.* **63**, 850 (1991).
2. D. G. Hafeman, J. W. Parce, H. M. McConnell, *Science* **240**, 1182 (1988).
3. J. W. Parce *et al.*, *ibid.* **246**, 243 (1989).
4. H. M. McConnell, P. Rice, H. G. Wada, J. C. Owicki, J. W. Parce, *Curr. Opin. Struct. Biol.* **1**, 647 (1991).
5. J. C. Owicki and J. W. Parce, *Biosens. Bioelectron.* **7**, 255 (1992).
6. For example, adrenergic agonists cause a significant decrease in acidification rate when added to the army worm ovary cell line Sf9 (B. Glaeser and S. Pitchford, personal communication).
7. The amplitude and kinetics of cell acidification response to receptor triggering depend on cell pretreatment. Because media frequently contain a variety of receptor ligands, the largest and most reproducible results are obtained with the use of cells that have been deprived of these factors for some period before the experiment. We have noted that when some cells are maintained in culture under normal growth conditions for extended periods of time, the amplitude and kinetics of the receptor-mediated acidification response can change. In contrast, cells maintained in the frozen state over extended periods give highly reproducible responses.
8. H. G. Wada *et al.*, *J. Cell. Physiol.*, in press.
9. In some experiments, it has been possible to separate in time acidification that is the result of receptor triggering and the onset of increased glycolytic rate through the sequential addition of receptor ligand and glucose.
10. C. M. Fraser, C. D. Wang, D. A. Robinson, J. D. Giocayne, J. C. Venter, *Mol. Pharmacol.* **36**, 840 (1989).
11. J. C. Owicki *et al.*, *Proc. Natl. Acad. Sci. U.S.A.* **87**, 4007 (1990).
12. G. T. Baxter *et al.*, unpublished results.
13. H. G. Wada, K. Fok, T. Nolan, W. Robinson, H. M. McConnell, paper presented at the National Institute of Allergy and Infectious Diseases Conference on Advances in Molecular Biology and Targeted Treatments for AIDS, Washington, DC, 14–18 May 1990.
14. B. Nag *et al.*, *J. Immunol.* **148**, 2040 (1992).
15. K. M. Raley-Susman, K. R. Miller, J. C. Owicki, R. M. Sapolsky, *J. Neurosci.* **12**, 773 (1992).
16. W. E. Holmes *et al.*, *Science* **256**, 1205 (1992).
17. P. Rice, thesis, Stanford University, Stanford, CA (1991).
18. D. L. Miller *et al.*, *FASEB J.* **5**, A1014 (1991).
19. J. W. Parce *et al.*, *Ann. Biol. Clin.* **48**, 639 (1990).
20. J. A. Salon *et al.*, *Soc. Neurosci. Abstr.* **17**, 86 (1991).
21. M. P. Rosser *et al.*, *ibid.*, p. 818.
22. P. A. Rice *et al.*, *FASEB J.* **5**, A1014 (1991).
23. S. R. Indelicato *et al.*, *Abstracts of the 5th International Conference on Immunopharmacology*, Tampa, FL, 27 to 30 May 1991.

24. We thank C. Venter and C. Fraser for helpful discussions concerning orphan receptors and P. Rice for some of the data in Fig. 3. Supported in part by the Defense Advanced Research Projects Agency, contract MDA972-92-C-0005.